

Technical Report: Multi-Carrier Position-Based Packet Forwarding in Wireless Sensor Networks*

Ahmed Bader and Karim Abed-Meraim

Telecom ParisTech, Paris, France

{bader,abed}@telecom-paristech.fr

Mohamed-Slim Alouini

KAUST, Thuwal, Mekkah Province, Saudi Arabia

slim.alouini@kaust.edu.sa

Abstract

Beaconless position-based forwarding protocols have recently evolved as a promising solution for packet forwarding in wireless sensor networks. However, as the node density grows, the overhead incurred in the process of relay selection grows significantly. As such, end-to-end performance in terms of energy and latency is adversely impacted. With the motivation of developing a packet forwarding mechanism that is tolerant to node density, an alternative position-based protocol is proposed in this paper. In contrast to existing beaconless protocols, the proposed protocol is designed such that it eliminates the need for potential relays to undergo a relay selection process. Rather, any eligible relay may decide to forward the packet ahead, thus significantly reducing the underlying overhead. The operation of the proposed protocol is empowered by exploiting favorable features of orthogonal frequency division multiplexing (OFDM) at the physical layer. The end-to-end performance of the proposed protocol is evaluated against existing beaconless position-based protocols analytically and as well by means of simulations. The proposed protocol is demonstrated in this paper to be more efficient. In particular, it is shown that for the same amount of energy the proposed protocol transports one bit from source to destination much quicker.

* This work was supported by Qatar National Research Fund (a member of Qatar Foundation).

I. INTRODUCTION

Wireless sensor networks (WSNs) are being increasingly considered for a multitude of monitoring and tracking applications in the fields of process automation, environmental monitoring, and tactical operations [1]. WSNs are not limited to terrestrial deployment scenarios but rather extend to submarine environments [2]. The WSN umbrella is also being expanded to fit more specific applications such as smart utility networks [3], [4] and multimedia applications [5]. The sincere interest in WSNs coupled with the wide spectrum of possible applications have created a tangible research surge across all layers of the protocol stack over the past decade. Yet, most research efforts tend to fine tune the balance between performance and cost. The most important factors influencing the design of WSNs are: energy, latency, complexity, and scalability [1], [6].

Packet forwarding is indeed one of the research issues which directly impacts all of the aforementioned design factors. Position-based forwarding protocols have emerged as some of the most efficient packet delivery solutions for WSNs [1]. This is mainly due to the fact that nodes can locally make their forwarding decisions using very limited knowledge of the overall network topology. However, classical position-based forwarding relies on periodical exchange of beacons in the form of location updates between neighboring nodes. Evidently, the beacon exchange process can often lead to a waste of bandwidth [7]. To alleviate this shortcoming, beaconless position-based forwarding techniques have evolved as being more efficient. Two of the earliest such protocols reported in literature are Geographic Random Forwarding (GeRaF) [8], [9] and Beaconless Routing (BLR) [10]. In beaconless position-based forwarding, potential relays undergo a distributed selection process whereby the node with the most favorable attributes (e.g. closeness to destination) shall eventually win the contention [7]. The sender of a packet first issues a request-to-send (RTS) message. Upon the reception of this message, potential relays lying within the sender's coverage zone enter into a time-based contention phase. Each potential relay triggers a timer whose expiry depends on a certain cost function. The first node to have its timer expire will transmit a clear-to-send (CTS) message on the next time slot. However, since time is slotted it is quite probable for collisions to occur. A secondary collision resolution phase will be required in that case.

The ideas presented in [8], [9] and [10] have been well-accepted within the research community and have been furthered and/or adapted in [11], [12], [13], [14], [15]. In Contention-Based

Forwarding (CBF) [11], response time to a RTS message is rather calculated as function of the advancement towards the destination. In [12], a protocol dubbed as Implicit Geographical Forwarding (IGF) is proposed. IGF utilizes residual energy and progress towards the destination as joint criteria for relay selection. On the other hand, MACRO [13] weighs the response time of potential relays with the progress that can be made per unit power. Authors of [14] propose a technique called Cost- and Collision-Minimizing Routing (CCMR) whereby contending relays dynamically adjust their cost metrics during the selection process. In [15], GeRaF is modified such that it serves wireless sensor networks with multiple sinks.

Beaconless position-based forwarding offered valuable improvements compared to their beacon-based predecessors. However, they are plagued by an overhead which rapidly grows with node density. As node density grows, collisions between candidate relays contending for medium are more probable to occur, and thus the overhead incurred grows noticeably. Not only does this degrade end-to-end delay performance, but it also increases the mean energy consumption. Furthermore, existing beaconless position-based protocols have been built and evaluated based on the classical “disc” coverage model. Under realistic multipath channel models, this causes frequent duplication of packets and obviously leads to the creation of co-channel interference [16].

In this paper, a novel position-based forwarding protocol is proposed. The protocol’s main virtue is that it does not resort to any relay selection process. At any given hop, potential relays check whether they satisfy certain position-based criteria. Any relay that *does satisfy* the criteria decides to forward the packet ahead. It does so without reverting to any sort of coordination with other potential relays. At the terminals of a receiving node, such a mechanism would undoubtedly create multiple copies of the same packet with different propagation delays. To remedy this problem, we utilize a physical layer (PHY) which is built over the use of orthogonal frequency division multiplexing (OFDM). By virtue of introducing a cyclic prefix (CP) to each OFDM symbol, a packet which is being simultaneously forwarded by multiple nodes can be correctly detected at a receiving node [17].

Early generations of WSNs have actually employed low-power Zigbee radios [18]. Zigbee is an IEEE specification utilizing Direct Sequence Spread Spectrum (DSSS) and is based on the IEEE 802.15.4 standard for wireless personal area networks (WPANs)[6]. Nevertheless, considering OFDM radios is a trend which has recently started to pick up and gain traction [19], [20]. The

adoption of OFDM (also often referred to as multi-carrier modulation) is mainly motivated by its ability to conveniently accommodate larger channel bandwidths while featuring less susceptibility to common radio channel impairments [17].

The idea of using OFDM for concurrent transmissions of the same packet has been actually proposed before in [21], [22]. Nevertheless, the work of [21], [22] was presented in the context of utilizing OFDM for efficiently flooding a message across the whole network. Obviously, this does not fit well into the WSN model where data from sensors must be efficiently disseminated to a very limited number of sinks. In the protocol presented in this paper, OFDM is combined with position-based relaying in order to streamline packets towards the intended destination.

The protocol presented herein is the fruit of the marriage between position-based relaying and OFDM. Nodes at a given hop i will decide to relay or not based on the positions of the source, the destination, and the relays of the previous hop, $i - 1$. OFDM on the other hand enables concurrent packet transmissions. The proposed protocol dedicates part of the OFDM time-frequency resources for a set of random access channel (RACH) slots. Each relay from the $(i - 1)$ th hop randomly selects one of the RACH slots and modulates it with its position information. When potential relays of the i th hop receive the packet, they will read the position information on all RACH slots and accordingly decide whether or not to relay. Obviously, it is probable that some RACH slots may be selected by more than one relay. Nonetheless, it will be demonstrated that such “collisions” on the RACH slots only affect the energy performance as well as the achievable hop distances. In other words, they do not impact the progression of the packet towards its destination. Furthermore, it will be shown that the proposed protocol improves the end-to-end delay performance when compared to existing beaconless schemes. However, the amount of end-to-end energy consumed is typically larger. This is due to the fact that one packet is concurrently transmitted by multiple nodes every hop. Interestingly, the improvement attained in terms of delay performance is sufficiently large to offset the impact of additional energy consumption. Indeed, this is the major contribution of this paper.

The rest of the paper is organized as follows. Section II offers an elaborate description for the operation of the protocol. Section III presents a model for the wireless channel and the physical layer. A detailed statistical analysis of the hopping behavior under the proposed protocol is given in section V. Evaluation of the end-to-end performance against existing beaconless position-based protocols and simulation results are provided in section VI. Finally, the main results are

summarized in section VII.

II. DESCRIPTION OF PROTOCOL OPERATION

Since the proposed protocol is built around the concept of utilizing OFDM, we will refer to it herein as OMR which is short of “OFDM-based Multihop Relaying”.

A. Key Assumptions

The following are key assumptions we used in the course of developing OMR:

- 1) Positions of packet sinks are known to all nodes. Packet sinks may periodically advertise their own positions to the rest of the network by means of a flooding process. In addition, all nodes have knowledge of their own positions. In the analysis, the source node V is located in the cartesian space at $(0, 0)$ while the destination Q is at $(L, 0)$.
- 2) Nodes are randomly distributed in the network according to a 2-D Poisson point distribution with density ρ . Furthermore, nodes implement a non-synchronized sleeping schedule with a duty cycle of ϵ .
- 3) If a node is awake but does not have data to transmit, then it will be in a state of channel acquisition. In this state, the node will be continuously monitoring the wireless medium for synchronization pilots so as to be able to lock to any nearby transmission / relaying process.
- 4) A decode-and-forward relaying strategy is adopted and nodes have omni-directional antennas.
- 5) Packet sinks are stationary. Nodes however can be fixed or mobile. For packet durations in the range of milliseconds, the node topology during one hop can be conveniently considered to stay unchanged even for speeds of up to 100 km/hr.
- 6) A busy tone is activated during listening and receiving to help mitigate the hidden node effect.

B. Packet Forwarding Process

In the sequel, we will describe in detail how a packet is relayed towards the destination. The source node V will first encode its own position information and that of the destination Q on two separate packet fields that are dedicated for this purpose. Figure 1 illustrates the proposed

packet structure for OMR. Each packet is appended by a CRC sequence. The source node then senses the wireless medium. The sensing activity must be performed on the data tones as well as the busy tone [8], [9], [23]. If there exists any ongoing transmission in the vicinity it backs off. Fixed window with binary exponential decrease back-off algorithms may be employed to maintain proportional fairness in the network [24]. If the medium is not busy, the source node will transmit the packet. Awaken nodes lying within the transmission range of the source node will first attempt to decode the packet and will activate the busy tone meanwhile. Nodes passing the CRC check will become part of the decoding set of the first hop denoted as \mathbf{D}_1 . As a notational standard in this paper, nodes in a given set are sorted in an ascending order according to their distance to the destination Q . Two position-based criteria are evaluated by each node in \mathbf{D}_1 . The first is proximity to the destination compared to the source. The second is whether it lies within a forwarding strip of width w surrounding the line between V and Q . The main objective of introducing the second criterion is to streamline the forwarding process into a certain geographical corridor. This will ensure that the interference created by the forwarding process is confined to a certain geographical region thus making more room for other forwarding processes. Nodes in \mathbf{D}_1 satisfying the two position-based criteria outlined above will become part of the relaying set \mathbf{R}_1 .

To proceed, nodes in \mathbf{R}_1 will have to convey their position information to nodes of the second hop. As shown in figure 1, the packet includes B RACH slots which are used for just that purpose. Each relay randomly selects one of those RACH slots to modulate its position information. Naturally, it is probable that one or more relays may choose the same RACH slot. In such a case, it will not be possible to resolve the position information of neither of those relays. Nodes of the second hop are able to pick up the position information of only those nodes in \mathbf{R}_1 which have selected unique RACH slots. Relays of the set \mathbf{R}_1 will transmit the packet after a small guard period. Awaken nodes which correctly receive this transmission will now form the set \mathbf{D}_2 . A node in \mathbf{D}_2 will decide to forward the packet if: it is inside the forwarding strip, and is closer to the destination than all nodes of \mathbf{R}_1 whose position information could be resolved. The forwarding process continues as described above for the next hops and is further illustrated by an example in figure 2.

The source gives each packet a unique identification (ID) label. Due to the sporadic nature of the wireless channel, a node may receive the same packet a second time. By means of the

unique ID, the node will be able to determine it is a duplicate packet and thus will decide to drop it. This should happen before it continues the decoding process, i.e. the node will not be part of the decoding set of nodes.

C. Effect of RACH Collisions

The number of relays at hop i is denoted by \tilde{K}_i such that $\mathbf{R}_i = \{R_{i,k}\}_{k=1}^{\tilde{K}_i}$. A RACH collision is defined within this context as the event of having two or more relays select the same RACH slot to modulate their position information. As such, next-hop nodes will not be able to resolve the positions of those relays. Recalling that \mathbf{R}_i is an ordered set, we define (j_i) to be the index of the first node in \mathbf{R}_i whose position is resolvable, i.e. the positions of the first $j_i - 1$ nodes are unresolvable. Accordingly, it is probable that some nodes at hop $i + 1$ may relay the packet even though they do not offer positive progress towards the destination. In other words, they may be farther from the destination compared to some or all of those $j_i - 1$ relays. This is best illustrated by an example. Looking at figure 2, node $R_{i,7}$ does not offer positive progress with respect to the node $R_{i-1,1} \in \mathbf{R}_{i-1}$. Nonetheless, $R_{i,7}$ will actually decide to relay since the position information of $R_{i-1,1}$ happens to be unresolvable. The first node in \mathbf{R}_{i-1} whose position is resolvable is $R_{i-1,j_{i-1}}$, where in this specific example $j_{i-1} = 2$. The relaying criteria described above can be formalized by first defining x_{C_i} as the arc extended from Q and passing through node $R_{i-1,j_{i-1}}$. Subsequently, a node in \mathbf{D}_i will relay the packet if it lies in the area $\oslash \{x_{C_i}, y = \pm \frac{w}{2}\}$. Throughout this paper we use the operator \oslash to denote the area confined between multiple contours.

D. Carrier Sense Multiple Access at the Source

We denote the number of nodes forming the decoding set at hop i by $\tilde{L}_i = |\mathbf{D}_i|$. During hop i , the back-off region produced by the forwarding process is composed of two subareas. The first one is governed by the activity on the data channel, i.e. the concurrent transmissions of \tilde{K}_{i-1} relays. The second subarea is actually dictated by the superposition of the busy tone signals from all \tilde{L}_i receiving nodes. As such, the back-off region is substantially larger than the coverage zone of a single node, e.g. a hidden node. Accordingly, relays in the case of OMR can drop the task of sensing the medium before accessing it. Channel sensing is only performed by the packet source node upon the injection of a brand new packet. In contrast, relays in existing beaconless

protocols cannot afford as much not to listen to the channel before transmitting. This is because the back-off region at the final stages of the relay selection cycle is dictated by only very few candidate relays. In other words, it will be only slightly larger than the interference zone of a hidden node. Therefore, the impact of a possible hidden node transmission is more drastically felt in the case of traditional beaconless protocols. It is worthwhile noting at this point that the hidden node issue has been implicitly overlooked in [10], [11], [12], [13], [14], [15]. On the other hand, it was ignored in [8] and [9] under the assumption of light to moderate traffic loads.

E. Retransmission Policy

For the purpose of making OMR more reliable, a retransmission policy must be devised. Nodes of \mathbf{R}_i will need to retransmit if the set \mathbf{R}_{i+1} is empty, i.e. if there are no nodes which decide to transmit the packet at hop $i + 1$. To detect this event, each relay in \mathbf{R}_i must listen to the wireless channel to verify that the packet is being forwarded ahead. A relay in \mathbf{R}_i will consider that the packet is being forwarded if it is able to detect that packet's ID during the listening phase. The packet ID is allocated a distinct field in the packet's header as shown in figure 1. For the sake of saving energy, relays do not continue listening beyond the packet ID time mark. Therefore, the listening activity only occurs for a limited duration denoted here as t_{ID} . Powerful error coding must be utilized for the packet ID field to make the listening task more robust.

Every time the packet is retransmitted, the width of the forwarding strip, w , is increased by adjusting the corresponding value in the packet header (figure 1). This reduces the probability that another retransmission would be required. An expression for the expected number of retransmissions at a given hop count is derived in section V and is given in equation (24). It is also plotted in figure 3(a) for various values of node density and transmit power. It is clear from the figure that the expected number of retransmissions probability decreases as the packet progresses towards the destination or as the node density increases. Similarly, retransmission is less likely to occur as the transmit power increases. Having described the retransmissions policy, we can now summarize all different protocol states along with corresponding state transitions in the diagram of figure 4.

F. False Alarm Retransmissions

A special case worthwhile investigating here is when a relay makes an erroneous retransmission decision. This happens if a packet is actually being forwarded ahead by nodes of \mathbf{R}_{i+1} , but a relay from \mathbf{R}_i believes otherwise, i.e. it was not able to detect the packet ID during the listening phase. In order to minimize the implications of a such a “false alarm” case, relays must retransmit the packet only after the full packet duration (denoted here by T_p) elapses. Moreover, the number of retransmissions must be also capped to avoid infinite retransmission loops by the false-alarm relay. If the number of retransmissions is capped at $n_{r_{max}}$, then the impact of a false-alarm retransmission event is only limited to incrementing the size of the relay sets $\{\mathbf{R}_{i+n}\}_{n=2}^{n_{r_{max}}+1}$ by one. We assume that the guard time of the OFDM symbol is in the range of $120\mu s$ similar to [19]. Consequently, for a false alarm retransmission to cause harmful interference, it has to lie more than 7.2 km away from the current hop. Typical dimensions of a WSN makes us easily conclude that it is quite unlikely for harmful interference to occur in the case of false-alarm retransmissions. Furthermore, in case of a dense network and highly redundant error coding of the packet ID, the false-alarm event becomes even more unlikely to occur. Indeed, this intuition is validated in figure 3(b). Accordingly, we are practically able to neglect false-alarm retransmissions in our subsequent analysis.

G. Miscellaneous

Finally, it is worthwhile mentioning that we have evaluated the potential of utilizing transmit diversity techniques for OMR. In particular, we have considered the use of randomized transmit codes [25] since they do not require relays to coordinate their precoding matrices. However, the implementation of such codes may prove to induce substantial overhead as they mandate long training sequences for proper channel estimation. Furthermore, they are suitable for the specific case of narrow-band fading channels but not necessarily for wideband channels.

III. PHYSICAL LAYER MODELING

In this section, a mathematical model for the overall channel response is presented. Furthermore, a condition for successful packet detection is developed.

A. Wireless Channel Model

The channel between an arbitrary pair of nodes is represented by a generic wideband multipath tap-delay line with Rayleigh-distributed tap gains [26] as shown in figure 5. On average, there are n_h such taps. Natural echoes due to multipath are grouped in intervals of duration of T seconds. The delays $T'_1, \dots, T'_{\tilde{K}_{i-1}}$ reflect the general case that the start of the \tilde{K}_{i-1} transmissions are not perfectly aligned in time. The duration of the OFDM symbol is assumed to be larger than $(n_h - 1)T + \max\{T'_k\}_{k=1}^{\tilde{K}_{i-1}} - \min\{T'_k\}_{k=1}^{\tilde{K}_{i-1}}$ ensuring that each subcarrier encounters approximately a frequency-flat fading [17]. Amending each OFDM symbols with a cyclic prefix eliminates inter-carrier interference (ICI) and restores orthogonality between subcarriers. This enables decoupled signal detection at each subcarrier. Given a certain packet is relayed at hop i by \tilde{K}_{i-1} nodes, then the frequency response of the total channel at subcarrier f_l is given by $H(f_l) = \sum_{k=1}^{\tilde{K}_{i-1}} e^{-j2\pi f_l T'_k} \sum_{n=1}^{n_h} h_{k,n} e^{-j2\pi f_l (n-1)T}$. It is assumed that the duration of the cyclic prefix of the OFDM symbol is long enough such that all signal echoes (natural and artificial) arrive within the cyclic prefix interval. Other ongoing packet relaying processes will rather contribute to the interference signal. This interference however will be also Gaussian since the individual channel gains are Gaussian [27]. The exact nature of such an external interference is beyond the scope of the present paper and is rather a subject of future work. Under the reasonable assumption that the fading coefficients $h_{k,n}$ are all mutually independent, it follows that $H(f_l)$ is complex Gaussian such that $H(f_l) \sim \mathcal{N}(0, \sigma_S^2)$. $|H(f_l)|^2$ is exponentially distributed with a mean of $2\sigma_S^2 = 2 \sum_{k=1}^{\tilde{K}_{i-1}} \sum_{n=1}^{n_h} \mathbb{E}[|h_{k,n}|^2]$. We note that $\sum_{n=1}^{n_h} \mathbb{E}[|h_{k,n}|^2]$ represents the mean power content of the channel between the receiver and the k th relay and is equal to $\left(\lambda/4\pi\sqrt{(x-x_k)^2 + (y-y_k)^2}\right)^\alpha$. Here λ represents the wavelength, α is the large-scale path loss exponent, and $\sqrt{(x-x_k)^2 + (y-y_k)^2}$ is the distance from the receiver located at (x, y) to the k th relay located at (x_k, y_k) . Therefore, we obtain

$$\sigma_S^2 = \left(\frac{\lambda}{4\pi}\right)^\alpha \sum_{k=1}^{\tilde{K}_{i-1}} \frac{1}{((x-x_k)^2 + (y-y_k)^2)^{\frac{\alpha}{2}}}. \quad (1)$$

Phase shift keying (PSK) modulation is utilized such that the transmit power is equal for all subcarriers. The signal to interference plus noise ratio (SINR) at subcarrier f_l is given by $\gamma(f_l) = \frac{P_t |H(f_l)|^2}{N_s P_n}$, where P_t is the transmit power over the whole bandwidth, N_s is the number of subcarriers, and P_n is the noise plus interference power within the subcarrier bandwidth. The

average SINR is subcarrier-independent and is denoted by $\gamma_o = \frac{2P_t}{N_s P_n} \sigma_S^2$.

B. Successful Packet Detection

The outage probability, P_o , is the probability that $\gamma(f_l) < \gamma_t$ and equals $1 - e^{-\gamma_t/\gamma_o}$. We consider that a packet is successfully detected if $P_o < \tau$, where τ is a detection reliability parameter [28]. The value of τ relies on the underlying coding and interleaving techniques¹. With $0 < \tau < 1$, and recalling that $\gamma_o = \frac{2P_t}{N_s P_n} \sigma_S^2$, then the condition for successful detection is expressed as

$$\sigma_S^2 \geq \frac{N_s P_n \gamma_t}{2P_t \ln \frac{1}{1-\tau}}. \quad (2)$$

The mean coverage contour for hop i is denoted by $x_{H_i}(y), |y| \leq \frac{w}{2}$. Based on the successful packet detection condition of (2) and in light of (1) we define

$$x_{H_i}(y) : H_i(x_{H_i}(y), y) = U, \quad (3)$$

where

$$\begin{aligned} H_i(x_{H_i}(y), y) &= \sum_{k=1}^{\tilde{K}_{i-1}} \frac{1}{((x_{H_i}(y) - x_k)^2 + (y - y_k)^2)^{\frac{\alpha}{2}}}, \\ U &= \frac{N_s P_n}{2P_t} \left(\frac{4\pi}{\lambda} \right)^\alpha \frac{\gamma_t}{\ln \frac{1}{1-\tau}}. \end{aligned}$$

For the first hop, we have $x_{H_1}(y) = \sqrt{\frac{1}{U^{\frac{2}{\alpha}}} - y^2}$.

IV. PRACTICAL CONSIDERATIONS

A. Timing Considerations

We recall our assumption that a fairly accurate clock and frequency synchronization between nodes is attained via the same process by which the position information is acquired [1]. In fact, the forwarding process itself may also aid to achieve the same goal by means of the synchronization pilots inserted in the packet header. Furthermore, if an external localization method such as the global positioning system (GPS) is used, then nodes can be also aligned to a universal time reference. However, GPS is known to be power-hungry and thus is generally

¹With reference to figure 1, it is assumed that interleaving is only applied to the payload and CRC portions of the packet. This will enable relays in the listening phase to drop right after the packet ID time mark.

unfavorable for WSNs. When other localization methods are utilized nevertheless, we must assume that a universal time reference does not generally exist. Instead, a node in the receiving state will align its time reference to the first energy arrival. As such, nodes within a decoding set D_i will generally have different time references. This concept is illustrated in figure 6. Non-aligned time references obviously results in asynchronous transmissions by relays. It is important at this point to study the implications of asynchronous relaying on the delay spread at the destination Q . For an arbitrary node $R_{i,k}$, the propagation delay of the 1st energy arrival with respect to the packet source is given by the following recursive formula

$$d_{p_{i,k}} = \min\{\overline{R_{i,k}R_{i-1,n}} + d_{p_{i-1,n}} + \delta_r\}_{n=1}^{\tilde{K}_{i-1}}. \quad (4)$$

In (4) we have expressed propagation delay in terms of distance rather than time for notational convenience. The term δ_r in Equation 4 represents the difference in length between the specular path and the first multipath echo of the Rayleigh channel. We recall that Rayleigh channels do not include a specular path. For the sake of simplicity, we assume that δ_r is approximately equal for all pairs of nodes selected from within two consecutive hops. The forwarding delay spread at the destination Q can then be expressed as

$$\max\{\overline{QR_{q-1,k}} + d_{p_{q-1,k}}\}_{k=1}^{\tilde{K}_{q-1}} - \min\{\overline{QR_{q-1,k}} + d_{p_{q-1,k}}\}_{k=1}^{\tilde{K}_{q-1}}. \quad (5)$$

The total delay spread is naturally the sum of the forwarding delay spread and the multipath delay spread. At the first glance, the discussion above may induce the impression that the forwarding delay spread may grow indefinitely as packets progress towards the destination. However, a closer look at the issue suggests otherwise. The first few relays to receive and then transmit the packet at hop i are typically those who are the *closest* to the $(i-1)$ th hop. At the same time, they are typically the *farthest* from the $(i+1)$ th hop and thus will have the largest propagation delays. It is straightforward to validate this intuition analytically for a linear network. In fact, it can be shown that for a linear network, packet copies are aligned in time every other hop, i.e. i is even. This is true when B is sufficiently large such that we may ignore the probability of having negative progress nodes. For 2-D networks however, it is quite more involved to validate such an intuition analytically. Rather it can be more conveniently verified through simulations. figure 7 illustrates the mean and standard deviation of the forwarding delay spread for strip widths between 100 and 200 meters. Simulations have been carried out for 3 different values

of node density, ρ . As can be inferred from the figure, the mean and standard deviation are almost independent of the node density. It is also shown that for this range of strip width, the mean is approximately $2\mu\text{s}$ with a standard deviation of no more than $0.35\mu\text{s}$. This is valuable information as it provides guidance on the suitable length of the cyclic prefix. For instance the length of the cyclic prefix in LTE is at least $4.7\mu\text{s}$ while it is $10\mu\text{s}$ for the IEEE 802.16e standard. Hence it is possible to utilize any of these two standardized OFDM radios for OMR. This is not the case for the IEEE 802.11g standards where the duration of the the cyclic prefix is only $0.8\mu\text{s}$. It can be further observed from figure 7(b) that the forwarding delay spread tends to follow a normal distribution. Moreover, figure 7(a) indicates that the standard deviation of the forwarding delay spread increases with the strip width, which is quite intuitive.

B. Effect of Time Offset on RACH Signals

The signal of a non-empty RACH slot is composed of the superposition of the location information of one or more relays. Each RACH slot is randomly picked by a unique set of relays. As such, each RACH signal undergoes a different channel towards a given receiver. Therefore, RACH signals are generally expected to be non-aligned in time, as exemplified in figure 8. Figure 8 is only showing first energy arrivals, i.e. subsequent signal echoes are not depicted. The RACH OFDM symbol is the aggregation of all the RACH signals. As shown in the figure, the receiver aligns its time reference to the first energy arrival of the first OFDM symbol. The FFT window is applied every integer multiple of the symbol duration. As a result, some RACH signals will be suffering from a time offset with respect to the start of the FFT window. The effect of time offset on the detection of OFDM symbols was studied in detail in [29]. It was shown in [29] that when the time offset is “towards” the CP, i.e. the FFT window is partially applied on the CP, then only a phase error is introduced. Interestingly, it is only time offsets towards the CP are possible in the case of OMR. If differential PSK is adopted, then the effect of the time offset is greatly marginalized.

V. STATISTICAL MODELING OF HOPPING DYNAMICS

In this section, an elaborate statistical framework is constructed for the sake of capturing the dynamics of packet hopping under OMR. We start off by recalling that given \tilde{K}_i relays in \mathbf{R}_i , then j_i represents the index of the 1st relay in \mathbf{R}_i whose position information is resolvable. Our next

goal is to derive an expression for the probability density function (PDF) $p_{j_i}(j_i|\tilde{K}_i)$. To proceed, we consider that the ordered set \mathbf{R}_i can be expressed as a block of length \tilde{K}_i constructed from the alphabet $\{0, 1\}$. Here “0” represents the event of being unresolvable while “1” represents the complementary event. Furthermore, we represent the “do not care” state with “x”. Accordingly, $p_{j_i}(j_i|\tilde{K}_i)$ is equivalent to $\mathbb{P}[R_{i,1}R_{i,2}\dots R_{i,j_i}\dots R_{i,\tilde{K}_i} = \underbrace{00\dots 01}_{j_i}x\dots x]$. To proceed, it is more convenient first to derive an expression for the probability $\mathbb{P}[R_{i,1}R_{i,2}\dots R_{i,j_i}\dots R_{i,\tilde{K}_i} = \underbrace{00\dots 0}_{j_i-1}x\dots x]$ which equals $1 - (\mathbb{P}[\underbrace{00\dots 01}_{j_i-1}x\dots x] + \mathbb{P}[\underbrace{00\dots 10}_{j_i-1}x\dots x] + \dots + \mathbb{P}[\underbrace{11\dots 11}_{j_i-1}x\dots x])$. Let us define $\mathfrak{B}^{(m)}(\cdot)$ as a decimal-to-binary conversion operator and $\mathfrak{C}^{(n,m)}(\cdot)$ as a cyclic shift right operator, where m corresponds to the size of the binary word and n is the order of the shift operator. It can be shown that the set represented by $\{\mathfrak{B}^{(j_i-1)}(k)\}_{k=1}^{2^{j_i-1}-1}$ is completely covered by

$$\{\mathfrak{C}^{(n,j_i-1)}(1x\dots x)\}_{n=0}^{j_i-2} - \{\mathfrak{C}^{(n,j_i-1)}(11x\dots x)\}_{n=0}^{j_i-3} + \dots (-1)^{j_i-1}\{\mathfrak{C}^{(0,j_i-1)}(11\dots 1)\}. \quad (6)$$

Furthermore, we define p_z as the probability of having exactly z relays in \mathbf{R}_i whose position information are resolvable. p_z can be evaluated recursively such that

$$p_z = \begin{cases} \left(\frac{B-1}{B}\right)^{\tilde{K}_i-1}, & z = 1 \\ p_{z-1} \left(\frac{B-z}{B-z+1}\right)^{\tilde{K}_i-z}, & z = 2 \dots B-2 \\ 0, & z \geq B-1 \end{cases} \quad (7)$$

Consequently, it follows from (6) and (7) that

$$\mathbb{P}[R_{i,1}R_{i,2}\dots R_{i,j_i}\dots R_{i,\tilde{K}_i} = \underbrace{00\dots 0}_{j_i-1}x\dots x] = 1 + \sum_{z=1}^{j_i-1} (-1)^z \binom{j_i-1}{z} p_z. \quad (8)$$

Now since $\mathbb{P}[R_{i,1}R_{i,2}\dots R_{i,j_i}\dots R_{i,\tilde{K}_i} = \underbrace{00\dots 01}_{j_i}x\dots x]$ is equal to $\mathbb{P}[R_{i,j_i} = 1]\mathbb{P}[R_{i,1}\dots R_{i,j_i-1} = 00\dots 0|R_{i,j_i} = 1]$, then we obtain

$$p_{j_i}(j_i|\tilde{K}_i) = \begin{cases} \left(\frac{B-1}{B}\right)^{\tilde{K}_i-1} \left(1 + \sum_{z=1}^{j_i-1} (-1)^z \binom{j_i-1}{z} p_z\right), & j_i = 1 \dots \tilde{K}_i \\ 1 + \sum_{z=1}^{\tilde{K}_i} (-1)^z \binom{j_i-1}{z} p_z, & j_i = 0 \end{cases} \quad (9)$$

where $j_i = 0$ refers to the event of all relays being unresolvable. The probabilities p_z and p_1 in (9) are re-evaluated by replacing B in (7) with $B-1$. Since $p_1 > \dots > p_{z-1} > p_z$, it can be shown that $\frac{dp_{j_i}(j_i|\tilde{K}_i)}{dB} < 0$, i.e. $p_{j_i}(j_i|\tilde{K}_i)$ decreases monotonically in B . This is intuitive since the number of RACH collisions is expected to decrease as B increases.

Another important modeling aspect is to characterize the mean coverage contour at each hop. From (3), it can be shown that $x_{H_i}(y)$, $|y| \leq \pm \frac{w}{2}$ is concave, i.e. $x_{H_i}(y)$ has a single maximum in $|y| \leq \pm \frac{w}{2}$. This indicates that $x_{H_i}(y)$ may be approximated by a circular arc. Furthermore, as w increases, so does \tilde{K}_{i-1} (on average). For two strip widths, w_1 and w_2 , where $w_2 > w_1$, we have $x_{H_i}(y, w_2) > x_{H_i}(y, w_1)$. This suggests that if $x_{H_i}(y)$ is to be approximated by an arc, then its radius depends on w and thus can be expressed as Ωw^c , where Ω and c are network-dependent constants. Indeed, the circularity of the coverage contour and the dependency of its radius on w have been validated numerically through a sufficient number of simulations. Those simulations have also revealed that the progress made every hop may be approximated by a linear function in \tilde{K}_{i-1} as demonstrated in figure 9. In other words, $\Delta x_{H_i}(y) = x_{H_i}(y) - x_{H_{i-1}}(y)$ is equivalent to $\varphi \tilde{K}_{i-1} + \beta x_{H_1}(0)$, where φ and β are network-dependent constants, and $x_{H_1}(0) = 1/U^{\frac{1}{\alpha}}$. Consequently, we get the following recursive relationship

$$x_{H_i}(y) = x_{H_{i-1}}(y) + \varphi \tilde{K}_{i-1} + \frac{\beta}{U^{\frac{1}{\alpha}}} = \varphi \sum_{n=1}^{i-1} \tilde{K}_n + (i-1) \frac{\beta}{U^{\frac{1}{\alpha}}} + x_{H_1}(y). \quad (10)$$

The intuition behind the linear approximation in (10) may be better perceived by considering the hypothetical case of having \tilde{K}_{i-1} co-located relays. In such a case, we have $x_{H_i}(y) = x_k + \sqrt{(\tilde{K}_{i-1}/U)^{2/\alpha} - (y - y_k)^2}$ using (3). It can be shown that a linear approximation here is good enough to provide a mean absolute percentage error (MAPE) of 5.5% (and as low as 3% for $\tilde{K}_{i-1} > 3$).

To further study the hopping behavior of OMR, we consider the problem setup shown in figure 10. For narrow strips (w/L relatively small), the decision contour $x_{C_i}(y)$ can be conveniently assumed to be axially centered around the line $y = 0$. We recall that for hop $i-1$, we denoted the 1st relay in \mathbf{R}_{i-1} whose position information is resolvable by $R_{i-1,j_{i-1}}$. We need to find an expression for the distance of $R_{i-1,j_{i-1}}$ away from the point $(x_{H_{i-1}}(0), 0)$ which is in return approximately equal to the distance $x_{H_{i-1}}(0) - x_{C_i}(0)$. The expectation of the distance to the n th nearest neighbor in a sector with angle ϕ was derived in [28] and is given by $\sqrt{\frac{2}{\phi \epsilon \rho} (n - 1 - \frac{\pi}{4})}$. With reference to figure 10, the sector angle ϕ can be approximated to extend from $(x_{H_{i-1}}(0), 0)$ to the intercepts of $x_{H_{i-1}}(y)$ with $|y| = \frac{w}{2}$. Thus, ϕ can be estimated to be quite close to π . Therefore we get

$$x_{C_i}(0) \approx x_{H_{i-1}}(0) - \sqrt{\frac{2}{\pi \epsilon \rho} \left(j_{i-1} - 1 - \frac{\pi}{4} \right)}. \quad (11)$$

We further define the following areas (where $|y| \leq \pm \frac{w}{2}$):

$$\mathcal{A}_{D_i} = \mathcal{O} \{x_{H_{i-1}}(y), x_{H_i}(y)\}, \quad (12)$$

$$\mathcal{A}_{R_i} = \mathcal{O} \{x_{C_i}(y), x_{H_{i-1}}(y), x_{H_i}(y)\}, \quad (13)$$

$$\mathcal{A}_{D_i}^- = \mathcal{O} \{x_{H_{i-3}}, x_{H_{i-1}}\}, \quad (14)$$

$$\mathcal{A}_{R_i}^- = \mathcal{O} \{x_{C_i}(y), x_{H_{i-1}}(y)\}. \quad (15)$$

Moreover, the number of relays able to decode the packet at its i th hop is denoted by $\tilde{L}_i = |\mathbf{D}_i|$. In fact, \tilde{L}_i is composed of two terms such that $\tilde{L}_i = L_i + L_i^-$. The terms L_i and L_i^- correspond to nodes lying in \mathcal{A}_{D_i} and $\mathcal{A}_{D_i}^-$ respectively. We note that L_i^- can be further broken down into two components. The first corresponds to the nodes in $\mathcal{O} \{x_{H_{i-2}}, x_{H_{i-1}}\}$ who were asleep at the time when \mathbf{R}_{i-2} began their transmission but woke up before the transmission ended. Whereas the second encompasses the nodes in $\mathcal{O} \{x_{H_{i-3}}, x_{H_{i-2}}\}$ who were asleep during the whole transmission duration of \mathbf{R}_{i-3} and only woke up before the transmission of \mathbf{R}_{i-2} ended. For simplification and conciseness of the subsequent analysis, we assume that the sleeping time is equal to T_p such that the second component will have a value of zero and thus (14) reduces to $\mathcal{A}_{D_i}^- = \mathcal{O} \{x_{H_{i-2}}, x_{H_{i-1}}\}$. Similarly, we can define $\tilde{K}_i = |\mathbf{R}_i|$ as $\tilde{K}_i = K_i + K_i^-$, where K_i and K_i^- are the relays lying in \mathcal{A}_{R_i} and $\mathcal{A}_{R_i}^-$ respectively. K_i^- represents the nodes lying in $\mathcal{A}_{R_i}^-$ who were asleep at the time when \mathbf{R}_{i-2} began their transmission but woke up before the transmission ended.

In order to evaluate the energy and delay performance, we need to evaluate the expectations $\mathbb{E}[\tilde{L}_i]$ and $\mathbb{E}[\tilde{K}_i]$. A suitable starting point is to study the statistical dependencies of the areas \mathcal{A}_{R_i} , \mathcal{A}_{D_i} , $\mathcal{A}_{D_i}^-$, and $\mathcal{A}_{R_i}^-$. Based on (10) and in light of (12), it is clear the statistics of \mathcal{A}_{D_i} are completely encompassed by \tilde{K}_{i-1} . Similarly, from (10), (11), and (13) it can be shown that the statistics of \mathcal{A}_{R_i} are dictated by j_{i-1} , $\{\tilde{K}_n\}_{n=1}^{i-2}$, and $\{\tilde{K}_n\}_{n=1}^{i-1}$. On the other hand, using (10) and (14), and recalling the assumption that the sleep time is equal to T_p it is evident that the statistics $\mathcal{A}_{D_i}^-$ can be equivalently represented by those of \tilde{K}_{i-2} . Finally, since $\mathcal{A}_{R_i}^-$ is confined by $x_{C_i}(y)$ and $x_{H_{i-1}}(y)$ then using (10), (11), and (15) the statistics of $\mathcal{A}_{R_i}^-$ are actually encompassed by j_{i-1} and $\{\tilde{K}_n\}_{n=1}^{i-2}$. Given $S_{i-v} = \sum_{n=1}^{i-v} \tilde{K}_n$ and based on the statistical dependencies exposed

above, we subsequently obtain

$$p_{L_i}(L_i) = \sum_{\tilde{K}_{i-1}} p_{L_i}(L_i|\mathcal{A}_{D_i}) p_{\tilde{K}_{i-1}}(\tilde{K}_{i-1}), \quad (16)$$

$$p_{K_i}(K_i) = \sum_{j_{i-1}} \sum_{S_{i-1}} \sum_{S_{i-2}} p_{K_i}(K_i|\mathcal{A}_{R_i}) p(j_{i-1}, S_{i-1}, S_{i-2}), \quad (17)$$

$$p_{L_i^-}(L_i^-) = \sum_{\tilde{K}_{i-2}} p_{L_i^-}(L_i^-|\mathcal{A}_{D_i}^-) p_{\tilde{K}_{i-2}}(\tilde{K}_{i-2}), \quad (18)$$

$$p_{K_i^-}(K_i^-) = \sum_{j_{i-1}} \sum_{S_{i-2}} p_{K_i^-}(K_i^-|\mathcal{A}_{R_i}^-) p(j_{i-1}, S_{i-2}). \quad (19)$$

To take one step ahead, the probability that a node in $\mathcal{A}_{D_i}^-$ or similarly in $\mathcal{A}_{R_i}^-$ was sleeping when \mathbf{R}_{i-2} started transmitting is $p_{wk} = 1 - \epsilon$. Recalling that nodes are dispersed in the field according to a 2-D poisson distribution, we obtain

$$p_{L_i}(L_i|\mathcal{A}_{D_i}) = \frac{1}{L_i!} (\epsilon \rho \mathcal{A}_{D_i})^{L_i} e^{-\epsilon \rho \mathcal{A}_{D_i}}, \quad (20)$$

$$p_{K_i}(K_i|\mathcal{A}_{R_i}) = \frac{1}{K_i!} (\epsilon \rho \mathcal{A}_{R_i})^{K_i} e^{-\epsilon \rho \mathcal{A}_{R_i}}, \quad (21)$$

$$p_{L_i^-}(L_i^-|\mathcal{A}_{D_i}^-) = \frac{1}{L_i^-!} (\epsilon \rho \mathcal{A}_{D_i}^- p_{wk})^{L_i^-} e^{-\epsilon \rho \mathcal{A}_{D_i}^- p_{wk}}, \quad (22)$$

$$p_{K_i^-}(K_i^-|\mathcal{A}_{R_i}^-) = \frac{1}{K_i^-!} (\epsilon \rho \mathcal{A}_{R_i}^- p_{wk})^{K_i^-} e^{-\epsilon \rho \mathcal{A}_{R_i}^- p_{wk}}. \quad (23)$$

We note that $p_{S_{i-2}}(S_{i-2}) = *_{n=2}^{i-2} (p_{S_{n-1}}(S_{n-1}), p_{\tilde{K}_n}(\tilde{K}_n))$, where $*$ is the convolution operator. The joint PDF $p(j_{i-1}, S_{i-2})$ is given by $\sum_{S_{i-1}=0}^{\infty} p(j_{i-1}, S_{i-1}, S_{i-2})$, where $p(j_{i-1}, S_{i-1}, S_{i-2})$ equals the product of $p_{j_{i-1}}(j_{i-1}|S_{i-1}, S_{i-2})$, $p_{S_{i-1}}(S_{i-1}|S_{i-2})$, and $p_{S_{i-2}}(S_{i-2})$. Furthermore, $p_{S_{i-1}}(S_{i-1}|S_{i-2})$ is nothing but $p_{\tilde{K}_{i-1}}(S_{i-1} - S_{i-2})$. Also, $p_{j_{i-1}}(j_{i-1}|S_{i-1}, S_{i-2})$ is equivalent to $p_{j_{i-1}}(j_{i-1}|S_{i-1} - S_{i-2})$ and can be computed by evaluating (9) at $i-1$ instead of i and substituting \tilde{K}_{i-1} with $S_{i-1} - S_{i-2}$. With $p_{K_i^-}(K_i^-|\mathcal{A}_{R_i}^-)$ and $p(j_{i-1}, S_{i-2})$ readily available, we are now able to compute $p_{K_i^-}(K_i^-)$ from (15), (19), and (23). On the flip side of the coin, $p_{K_i}(K_i)$ can be computed from (13), (17), and (21) knowing that the joint PDF $p(j_{i-1}, S_{i-1}, S_{i-2})$ has already been computed above. Since $\tilde{K}_i = K_i + K_i^-$, then $p_{\tilde{K}_i}(\tilde{K}_i) = p_{K_i}(K_i) * p_{K_i^-}(K_i^-)$. From the statistical analysis presented thus far, it becomes clear that the statistics at any arbitrary hop can be conveniently obtained by recursion. In other words, at hop i , $p_{\tilde{K}_{i-1}}(\tilde{K}_{i-1})$ and $p_{\tilde{K}_{i-2}}(\tilde{K}_{i-2})$ will be readily available. Accordingly, $p_{L_i}(L_i)$ is obtained from (12), (16), and (20) while $p_{L_i^-}(L_i^-)$ is obtained from (14), (18), and (22).

Finally, we are in a position now to derive an expression for the expected number of re-transmissions $\mathbb{E}[n_{r_i}]$ occurring at hop i . Given the areas \mathcal{A}_{R_i} and $\mathcal{A}_{R_i}^-$, then $\mathbb{E}[n_{r_i}|\mathcal{A}_{R_i}, \mathcal{A}_{R_i}^-] = 1/(e^{\epsilon\rho(\mathcal{A}_{R_i} + p_{wk}\mathcal{A}_{R_i}^-)} - 1)$. If the number of RACH slots B is sufficiently large, then the contribution of $\mathcal{A}_{R_i}^-$ diminishes and may be overlooked in this expression for convenience and tractability of the analysis. Hence, we get:

$$\mathbb{E}[n_{r_i}] = \sum_{j_{i-1}} \sum_{S_{i-1}} \sum_{S_{i-2}} \mathbb{E}[n_{r_i}|\mathcal{A}_{R_i}] p(j_{i-1}, S_{i-1}, S_{i-2}). \quad (24)$$

VI. PERFORMANCE EVALUATION

To appreciate the end-to-end performance of OMR against other beaconless protocols, we are going to evaluate it in light of the inherent tradeoff between energy and delay. Denoting the mean end-to-end energy consumed in forwarding one packet by E_{e2e} and the mean end-to-end delay by l_{e2e} , we define the end-to-end energy-delay product as $\text{EDP} = E_{e2e}l_{e2e}$. In order to account for the fact that OMR and beaconless protocols may employ different modulation and coding schemes (MCS), EDP must be normalized by the PHY data rate, r . Hence, we can define an end-to-end cost metric $C_{e2e} = \frac{\text{EDP}}{rT_p}$ which reflects the amount of energy consumed and delay time spent in transporting rT_p bits from source to destination.

A. OMR Performance Metrics

At any given hop i , there would be \tilde{K}_{i-1} nodes who are relaying the packet and \tilde{L}_i nodes receiving the transmission. At the next hop, $i+1$, the \tilde{K}_{i-1} relays would be listening to make sure the packet is being forwarded ahead. Consequently,

$$l_{e2e} = T_p \sum_{i=1}^q (1 + \mathbb{E}[n_{r_i}]), \quad (25)$$

where $q : x_{H_q}(0) \geq L$ is the number of hops traversed by the packet to the destination. Furthermore, the energy expended at hop i to relay the packet ahead is given by:

$$\begin{aligned} E_i = & \mathbb{E}[\tilde{L}_i]P_{Rx}T_p + (\mathbb{E}[n_{r_i}] + 1)\mathbb{E}[\tilde{K}_{i-1}]P_tT_p + \\ & (\mathbb{E}[n_{r_i}] + 1)\mathbb{E}[\tilde{K}_{i-1}]P_{Rx}t_{ID} + (\mathbb{E}[\tilde{K}_{i-1}]t_{ID} + \mathbb{E}[\tilde{L}_i]T_p)\frac{P_t}{N_s}, \end{aligned} \quad (26)$$

where P_{Rx} is the power consumed in receiving a packet and $\frac{P_t}{N_s}$ is the busy tone power. The end-to-end energy consumed is $E_{e2e} = \sum_{i=1}^q E_i$.

B. A Spotlight on the Performance of Beaconless Protocols

The family of beaconless position-based forwarding protocols includes quite a few variants. Nevertheless, the work of [8], [9] constituted a major stepping stone towards the development of other beaconless protocols. In addition, the analytical framework provided in [8], [9] is quite comprehensive and detailed. As such, it is going to be adopted in this paper as the benchmark for comparison. Other beaconless protocols may be considered to a great extent as adaptations and/or enhancements of [8], [9]. Thus, evaluation results of this section can be conveniently generalized to other beaconless protocols. For the sake of brevity, we will be often using the term “BCL” to refer to the class of existing beaconless position-based protocols. Table I explains the different stages of the BCL forwarding process. At a given hop, there would be η empty cycles followed by one non-empty cycle. Empty cycles occur when there are no awoken nodes offering positive progress within the transmission range of the sender. The transmission range of the sender is denoted by d_m . On average, the fraction of nodes within the transmission range offering positive progress towards the destination is ξ . Each cycle consists of N_p slots such that the duration of one slots is T_s . For the non-empty cycle, there would be m_e empty slots followed by m_n collision-resolution slots. Summing up all terms of energy consumption, the mean energy consumed in transmitting one packet at a certain hop is given by

$$P_t T_s ((\mathbb{E}[m_e] + 5 + \mathbb{E}[\eta] N_p) N_s + (1 + 2\mathbb{E}[m_e] \xi) \epsilon \rho \pi d_m^2 + 1 + \mathbb{E}[m_e] + \mathbb{E}[\eta] N_p + \xi N_s \epsilon \rho \pi d_m^2 / N_p + (2 + 3N_s)(\mathbb{E}[m_n] - 1)) / N_s. \quad (27)$$

On the other hand, the mean energy consumed in receiving:

$$P_{Rx} T_s ((1 + 2\xi \mathbb{E}[m_e]) \epsilon \rho \pi d_{max}^2 + 2 + \mathbb{E}[m_e] + \mathbb{E}[\eta] N_p + 3(\mathbb{E}[m_n] - 1)). \quad (28)$$

The expectations $\mathbb{E}[\eta]$, $\mathbb{E}[m_e]$, and $\mathbb{E}[m_n]$ are found in explicit forms in [8] ((3) and (4)). The end-to-end delay is function of the time spent per hop and the number of hops traversed before reaching the destination. In light of table I, and [8] ((4), (5), and (16)), it can be shown that the time spent on average by a packet in the case of average beaconless protocols is given by $2(\mathbb{E}[\eta] N_p + \mathbb{E}[m_e + m_n]) T_s$. Furthermore, the expected progress towards the destination after i hops is given by [9], ((8) and (19)).

C. OMR vs. BCL

OMR performance was evaluated from an analytical point of view in light of the framework provided in Section V. It was then compared to [8], [9]. Furthermore, simulations have been carried out to validate the outcomes of the analytical computations. The strip width w was set to 200 m in the simulations with a source-destination separation of 2 km. The sleeping duty cycle was set to $\epsilon = 25\%$ while the detection threshold γ_t was assumed to be 5 dB at $\tau = 20\%$. The path loss exponent was considered to be $\alpha = 3$.

The main theme to be conveyed in this section, is that OMR starts to strikingly outperform existing beaconless position-based protocols in terms of end-to-end delay as node density grows. However, this comes at the price of additional energy consumption since a larger number of nodes tend to relay the packet. This reasserts the significance of evaluating end-to-end performance based on the interaction between energy and delay. We are going to show in this section that there is more than one scenario whereby OMR outperforms BCL protocols from the joint perspective of delay and energy. For instance, it will be demonstrated that by tuning down the transmit power of OMR, delay performance is not substantially impacted while energy consumption is noticeably reduced. Thus, OMR is able to provide an obvious performance gain in this case. Moreover, OMR will be also shown to have an edge for certain classes of modulation techniques. Finally and before delving into the detailed comparison, it ought to be mentioned that the outcome of analytical computations have been closely matched by simulation results, as per figure 11.

1) Effect of Transmit Power: It is clearly demonstrated from figure 11 that for an equivalent amount of energy consumption, OMR offers reduced end-to-end delay. This conclusion is mainly valid when OMR utilizes a lower transmit power. We have reverted to using a lower transmit power for OMR based on the rationale that it reduces energy consumption significantly while not really jeopardizing the hop distances traversed by packets. This argument stems from the simple fact that the relationship between the transmit power and the achievable hop distance is inversely scaled by the path loss exponent α . As such, a substantial drop in transmit power will be countered by only moderate to marginal shrink in hop distance, depending on the value of α . Indeed, this has been verified by plotting the ratio $C_{e2e}(\text{OMR})/C_{e2e}(\text{BCL})$ against OMR's transmit power for various node densities. Results are depicted in figure 12(a) which illustrates that OMR offers roughly a 40% enhancement when the transmit power is in the range of 6

to 9 dB below that of BCL (which is operating here at 33 dBm). Nevertheless, reducing the transmit power further below a certain threshold will actually start to have a counter effect. As the transmit power decreases, the probability of retransmission starts to pick up quickly and rather contributes to the inflation of OMR's EDP. It can be also concluded from figure 12(a) that the performance gains offered by OMR is almost indifferent of the underlying node density. Indeed, this is a design objective which has been set forth early on in this paper.

Since OMR does not resort to any collision resolution mechanism, it is also of interest to investigate the effect of the RTS/CTS packet duration, denoted by T_s , relative to the data packet duration, T_p . As T_s/T_p increases, a considerable portion of the end-to-end energy consumption in the beaconless case is attributed to RTS/CTS transmissions during the collision resolution process. End-to-end delay as well increases. Figure 12(b) illustrates that for shorter packet lengths, or alternatively larger T_s/T_p ratios, OMR is set to offer substantial performance gains over beaconless protocols.

2) *Effect of The Number of RACH Slots, B* : For the sake of a comprehensive and fair comparison, we have also studied the impact of B on the performance of OMR. On one hand, increasing B will reduce the probability of RACH collisions. This in return will have the effect of reducing the size of the area $\mathcal{A}_{R_i}^-$ and thus will result in reducing energy consumption. The delay performance will not be affected noticeably since the size of $\mathcal{A}_{R_i}^-$ is typically small compared to \mathcal{A}_{R_i} . On the other hand, as B gets larger, the overhead at the PHY layer also grows effectively resulting in a reduction of the effective data rate seen at layer 2. This intuition is indeed validated in figure 13(a).

3) *Higher Order MCS*: The performance gains demonstrated thus far are actually encouraging to consider a higher order MCS for OMR. We recall here our original choice to deploy a differential modulation scheme in conjunction with OMR. Whereas coherent modulation necessitates accurate estimation of the channel fading coefficients, differential modulation does not; thus reducing cost and complexity of the receiver. The tradeoff however in using M-DPSK instead of coherent M-PSK is a higher detection threshold. Now, our next task would be to specify the detection threshold γ_t for each MCS under consideration for OMR. The bit error rate (BER) targeted here is 10^{-2} . Under the assumption of two-branch maximal ratio combining (MRC) and Gray encoding, then the detection thresholds for DQPSK, 8-DPSK, and 16-DPSK

are approximately 12.8 dB, 15.6, and 18.5 dB respectively [30]. There is no need to consider 2-DPSK as it has the same detection threshold of DQPSK. On the other hand, for coherent QSPK, the required detection threshold at BER of 10^{-2} approximately evaluates to 10.85 dB [30]. Furthermore, if rate $\frac{1}{2}$ convolutional coding with a constraint length of 2 is employed then a coding gain of 3 to 4 dB can be achieved (at a BER of 10^{-2}) [31]. Figure 13(b) depicts the end-to-end cost incurred by OMR in comparison to BCL for various MCSs. BCL is assumed to use coherent QPSK. Figure 13(b) clearly conveys that OMR is able to transport the same amount of bits much faster while consuming the same amount of energy. Looking at it from a complementary angle, OMR delivers more bits towards the destination (by utilizing a higher order MCS) while consuming the same amount of energy and spending the same amount of delay.

Finally, simulations have been also carried out to investigate the behavior of OMR in case of forwarding two concurrent but dissimilar packets. A sample forwarding process is depicted in figure 14 noting that both packets have the same destination. Interference between the two forwarding processes has been accounted for in the simulation. It can be observed that one retransmission has occurred at the 4th hop of Packet A. This was due to the significant interference induced by the forwarding process of Packet B. As Packet B progressed further towards the destination, the forwarding process of Packet A gained some room to resume.

VII. CONCLUSIONS

In this paper we have proposed a novel multi-relay beaconless position-based packet forwarding protocol for WSNs. The protocol couples the use of an OFDM-based PHY with position-based routing to create an improved end-to-end performance over traditional beaconless protocols. A statistical framework has been provided to study the hopping dynamics and behavior of the proposed protocol. Numerical and simulation results have shown that the proposed protocol may be tuned to offer an improvement of up to 40% in terms of the end-to-end performance.

In our future work, we will study the applicability and performance of OMR in case of using the hop count away from the destination instead of geographical positions. We will also analyze the co-channel interference created by one forwarding process on another, evaluate how it limits the overall network capacity, and research means to control it.

REFERENCES

- [1] J. Yick, B. Mukherjee, and D. Ghosal, "Wireless sensor network survey," *Elsevier Journal on Comp. Net.*, vol. 58, Issue 12, pp. 2292–2330, April 2008.
- [2] I. Akyildiz, D. Pompili, and T. Melodia, "Underwater acoustic sensor networks: research challenges," *Elsevier Journal on Ad Hoc Networks*, vol. 3, no. 3, pp. 257–279, May 2005.
- [3] V. Gungor, B. Lu, and G. Hancke, "Opportunities and Challenges of Wireless Sensor Networks in Smart Grid," *IEEE Transactions on Industrial Electronics*, vol. 57, no. 10, pp. 3557–3564, October 2010.
- [4] M. Hatler, D. Phaneuf, and D. Gurganious, "Wireless Sensor Networks for Smart Cities: A Market Study," *ON World Research Report*, 2007.
- [5] I. Akyildiz, T. Melodia, and K. Chowdhury, "A survey on wireless multimedia sensor networks," *Elsevier Journal on Computer Networks*, vol. 51, no. 4, pp. 921–960, March 2007.
- [6] I. Akyildiz and M.C. Vuran, *Wireless Sensor Networks*, John Wiley and Sons, Ltd, 1st edition, 2010.
- [7] J. Sanchez, P. Ruiz, and R. Marin-Perez, "Beacon-less geographic routing made practical: Challenges, design guidelines, and protocols," *IEEE Communications Magazine*, vol. 47, Issue 8, pp. 85–91, August 2009.
- [8] M. Zorzi and R. Rao, "Geographic random forwarding (GeRaF) for ad hoc and sensor networks: Energy and latency performance," *IEEE Transactions on Mobile Computing*, vol. 2, no. 4, pp. 349–365, October 2003.
- [9] M. Zorzi and R. Rao, "Geographic random forwarding (GeRaF) for ad hoc and sensor networks: Multihop performance," *IEEE Transactions on Mobile Computing*, vol. 2, no. 4, pp. 337–348, October 2003.
- [10] M. Heissenbüttel, T. Braun, T. Bernoulli, and M. Wälchli, "BLR: beacon-less routing algorithm for mobile ad hoc networks," *Elsevier Journal on Computer Communications*, vol. 27, Issue 11, 2004.
- [11] H. Füssler, J. Widmer, M. Käsemann, M. Mauve, and H. Hartenstein, "Contention-based forwarding for mobile ad-hoc networks," *Elsevier Ad Hoc Networks*, vol. 1, Issue 4, pp. 351–369, November 2003.
- [12] T. He, B. Blum, Q. Cao, J. Stankovic, S. Son, and T. Abdelzaher, "Robust and timely communication over highly dynamic sensor networks," *Real-Time Systems*, vol. 37, No. 3, August 2007.
- [13] D. Ferrara, L. Galluccio, A. Leonardi, G. Morabito, and S. Palazzo, "MACRO: an integrated mac/routing protocol for geographic forwarding in wireless sensor networks," *In Proceedings of The 24th Annual Joint Conference of the IEEE Computer and Communications Societies (INFOCOM'05), Miami, USA*, vol. 3, pp. 1770–1781, March 2005.
- [14] M. Rossi, N. Bui, and M. Zorzi, "Cost- and collision-minimizing forwarding schemes for wireless sensor networks: Design, analysis and experimental validation," *IEEE Trans. on Mobile Computing*, vol. 8, No. 3, Mar 2009.
- [15] A. Odorizzi and G. Mazzini, "M-GeRaF analysis: Performance improvement of a multisink ad hoc and sensor network geographical random routing protocol," *In proceedings of 16th International Conference on Software, Telecommunications and Computer Networks (SoftCom 2008), Dubrovnik, Croatia*, pp. 193–197, September 2008.
- [16] M. Heissenbüttel, T. Braun, M. Wälchli, and T. Bernoulli, "Evaluating the limitations of and alternatives in beaconing," *Elsevier Journal on Ad Hoc Networks*, vol. 5, Issue 5, pp. 558–578, July 2007.
- [17] H. Schulze and C. Lueders, *Theory and Applications of OFDM and CDMA*, John Wiley and Sons Ltd, 1st edition, 2005.
- [18] P. Baronti, P. Pillaia, V. Chook, S. Chessa, A. Gotta, and Y. Fun Hu, "Wireless sensor networks: A survey on the state of the art and the 802.15.4 and ZigBee standards," *Elsevier Journal Computer Communications*, vol. 30, no. 7, pp. 1655–1695, May 2007.
- [19] E. Monnerie, J. Buffington, S. Shimada, and K. Waheed, "IEEE 802.15.4g OFDM PHY Overview," *doc. IEEE 802.11-10/1305r1*, January 2011.

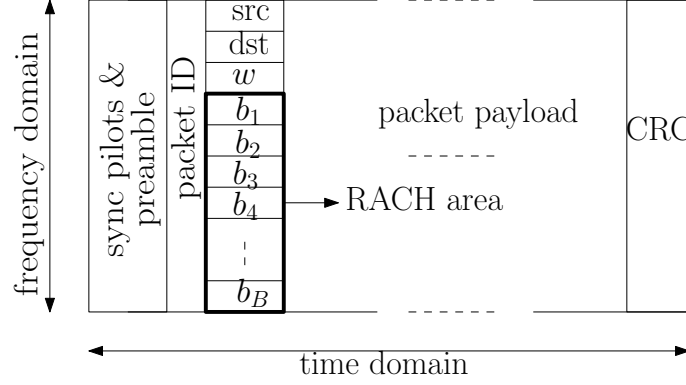


Fig. 1. OMR packet structure.

- [20] D. Wu, G. Zhu, D. Zhao, and L. Liu, "Energy Balancing in an OFDM-Based WSN," *IEEE 73rd Vehicular Technology Conference (VTC Spring)*, 2011.
- [21] M. Eriksson and A. Mahmud, "Dynamic single frequency networks in wireless multihop networks - energy aware routing algorithms with performance analysis," *In proceedings of The 10th IEEE International Conference on Computer and Information Technology, Bradford, UK*, pp. 400–406, May 2010.
- [22] M. Eriksson and A. Mahmud, "Transmitter macrodiversity in multihopping - SFN based algorithm for improved node reachability and robust routing," *World Academy of Science, Engineering and Technology*, vol. 64, 2010.
- [23] Z. J. Haas and J. Deng, "Dual busy tone multiple access (dbtma) - a multiple access control scheme for ad hoc networks," *IEEE Transactions on Communications*, vol. 50, no. 6, pp. 975–985, 2002.
- [24] I. Akyildiz, W. Su, Y. Sankarasubramaniam, and E. Cayirci, "Wireless sensor networks: A survey," *Elsevier Journal on Computer Networks*, vol. 38, Issue 4, pp. 393–422, January 2002.
- [25] A. Scaglione, D. Goeckel, and J. Laneman, "Cooperative Communications in Mobile Ad Hoc Networks," *IEEE Signal Processing Magazine*, vol. 23, Issue 5, pp. 18–29, September 2006.
- [26] T. Rappaport, *Wireless Communications: Principles and Practice*, Prentice Hall, 2nd edition, 2001.
- [27] B. Zhao and M.C. Valenti, "Practical relay networks: a generalization of hybrid-arq," *IEEE Journal on Selected Areas in Communications*, vol. 23, Issue 1, January 2005.
- [28] M. Haenggi, "On routing in random Rayleigh fading networks," *IEEE Transactions on Wireless Communications*, vol. 4, no. 4, April 2005.
- [29] C. Athaudage, "BER sensitivity of OFDM systems to time synchronization error," *The 8th International Conference on Communication Systems (ICCS'02), Singapore*, vol. 1, pp. 42–46, November 2002.
- [30] M. Simon and M.S. Alouini, *Digital Communication over Fading Channels*, John Wiley and Sons, 2nd edition, 2005.
- [31] Y. Yasuda, K. Kashiki, and Y. Hirata, "High-Rate Punctured Convolutional Codes for Soft Decision Viterbi Decoding," *IEEE Transactions on Communications*, vol. 32, no. 3, pp. 315–319, March 1984.

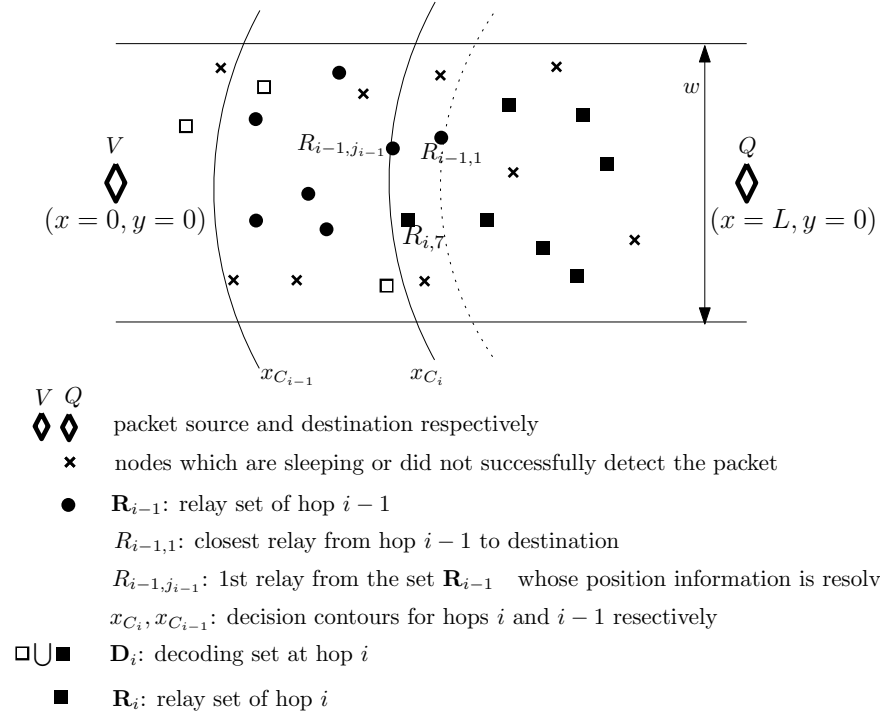
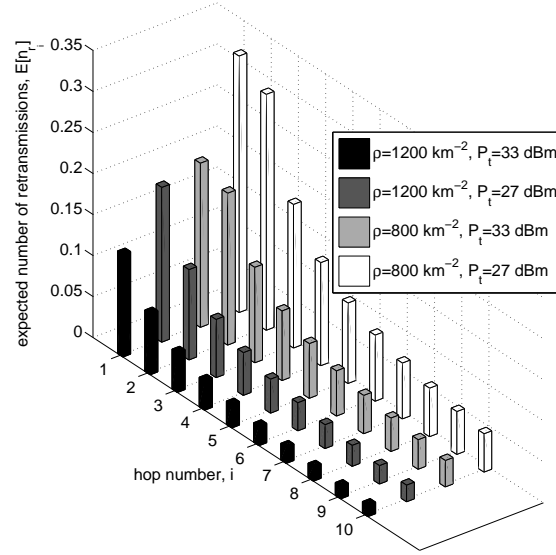
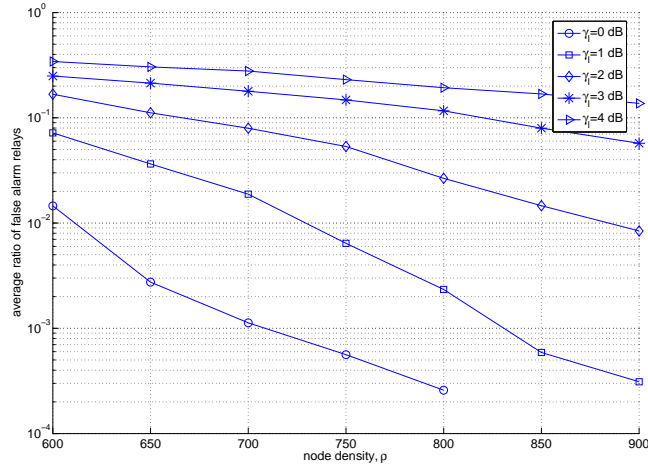


Fig. 2. Example of a sample hopping process.



(a) Expected number of retransmissions.



(b) Rate at which false alarm events occur for various values of the Packet ID decoding threshold. As more coding redundancy is associated with the Packet ID field, a lower threshold will be required.

Fig. 3. Evaluation of the proposed retransmission policy.

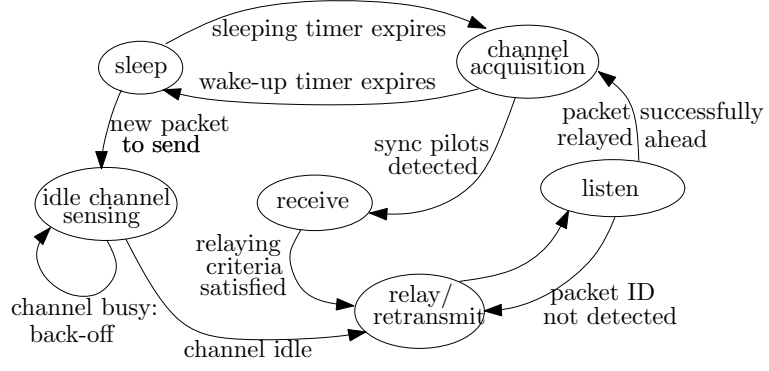


Fig. 4. Simplified protocol state diagram.

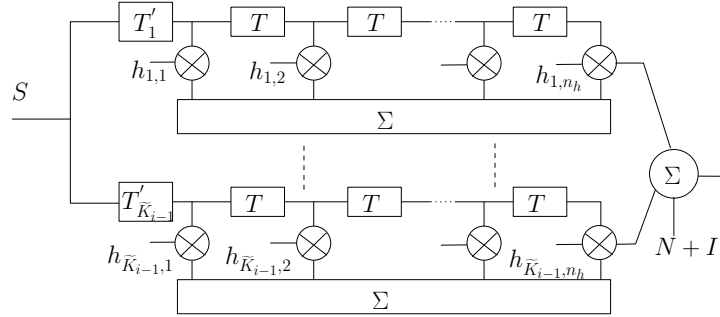
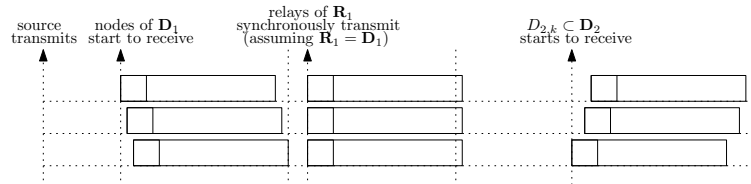
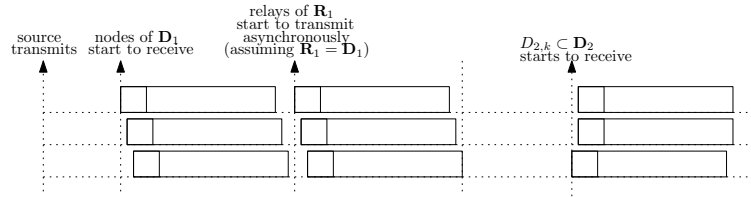


Fig. 5. Wireless channel model.

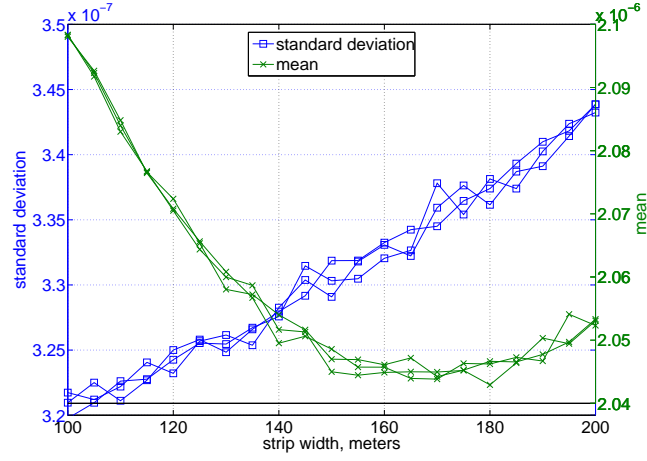


a) universal time reference, synchronous transmissions.

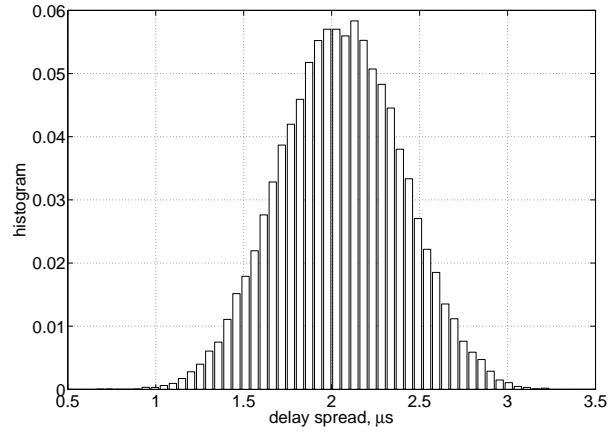


b) local time references, asynchronous transmissions.

Fig. 6. When universal time reference is available in the network by means of GPS for example, synchronous relaying is possible at each hop. A more general case however is to have asynchronous transmissions.



(a) Standard deviation and mean of the forwarding delay spread as function of the strip width for various node densities ($\rho = 900, 1200$, and 1500 km^{-2}). The length of the strip is 600m.



(b) Delay spread histogram ($\rho = 1500 \text{ km}^{-2}$, $w = 200\text{m}$, 50000 iterations).

Fig. 7. Statistics of the forwarding delay spread obtained through simulations.

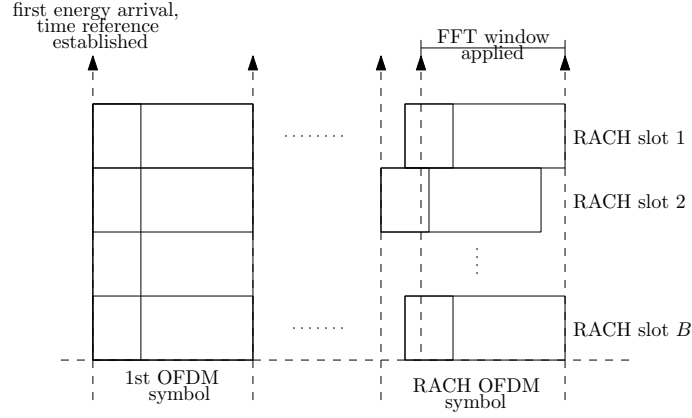


Fig. 8. For some RACH slots the FFT window will not be aligned to the actual start of the RACH signal.

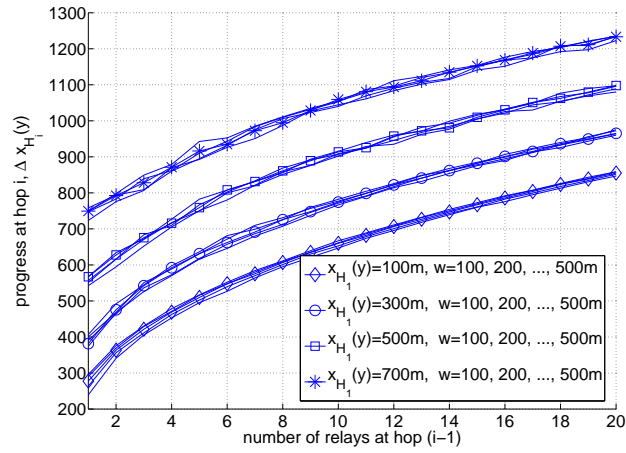


Fig. 9. Simulation results demonstrating that the progress made every hop is linear in \tilde{K}_{i-1} . The impact of the progress made in the 1st hop, $x_{H_1}(y)$, carries on to the subsequent hops. In other words, the larger $x_{H_1}(y)$ is, the greater progress is achieved in subsequent hops.

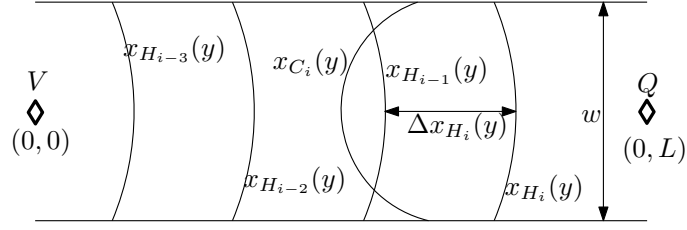


Fig. 10. Setup to study hopping behavior of OMR.

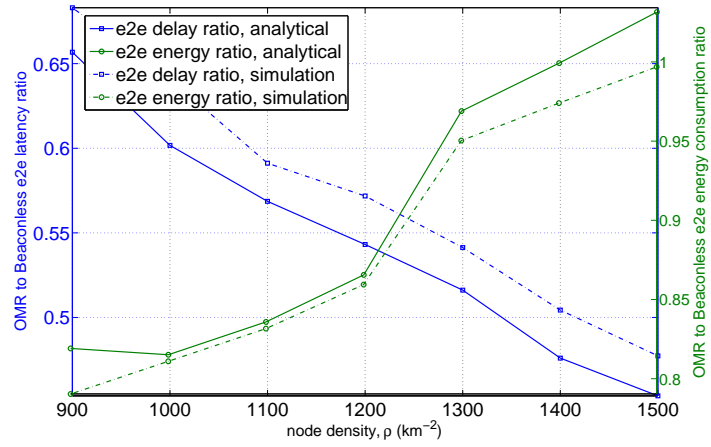
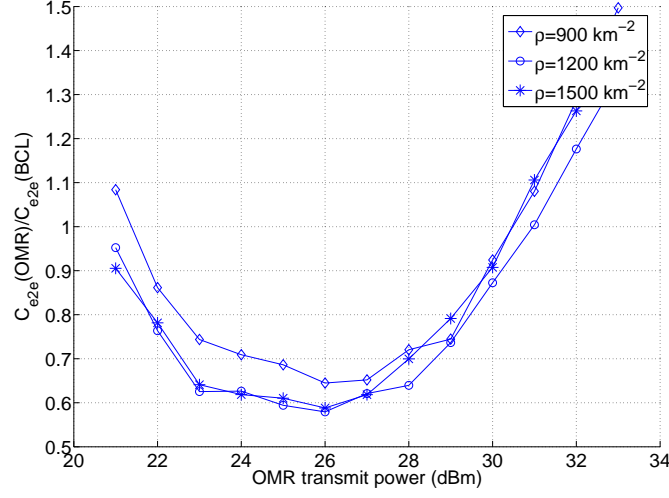
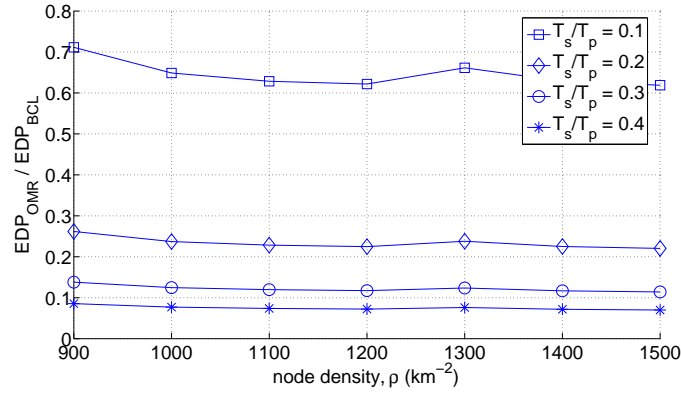


Fig. 11. End-to-end energy and delay performance of OMR compared to beaconless protocols. OMR is utilizing here a transmit power that is 9 dB less than beaconless.

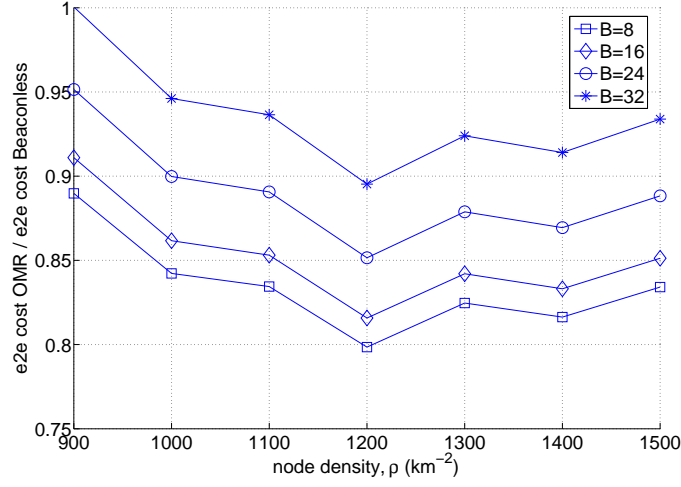


(a) End-to-end cost comparison as function of OMR transmit power at various node densities.

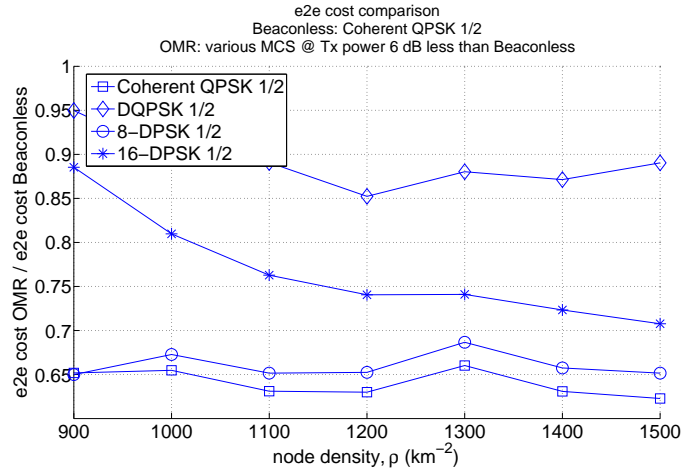


(b) End-to-end energy-delay product of OMR divided by that of the beaconless protocol. The duration of the control packet (RTS, CTS, ...) utilized by the beaconless protocol has been varied to study its impact on the performance. Here, OMR is operating at a transmit power which is 9 dB less than that of the beaconless.

Fig. 12. Comparing performance of OMR from and end-to-end perspective to beaconless protocols.

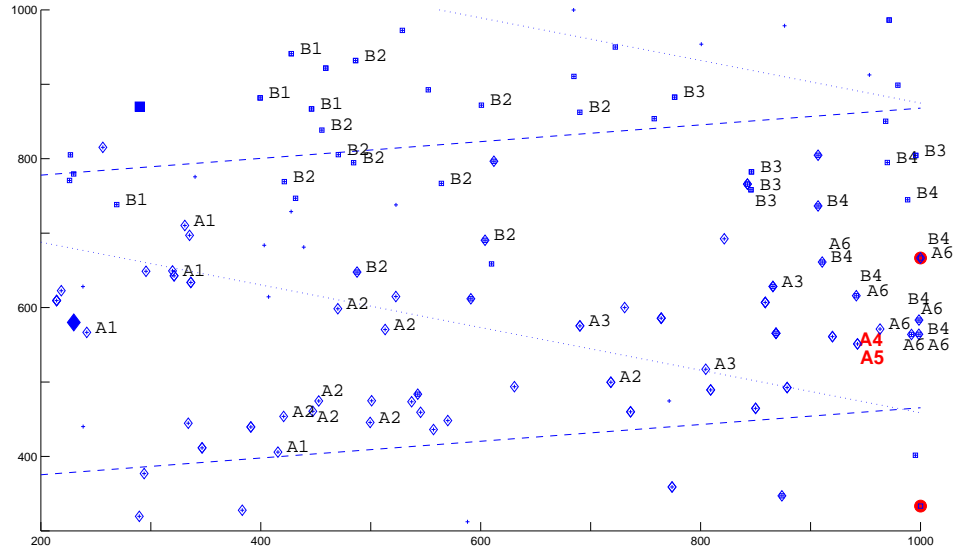


(a) End-to-end cost of OMR at various values of B (number of RACH slots) divided by that of the beaconless protocol.



(b) End-to-end cost of OMR at various modulation schemes divided by that of the beaconless protocol.

Fig. 13. Comparing performance of OMR from and end-to-end perspective to beaconless protocols, continued.



(a) Snapshots of two concurrent packet relaying processes

- | | | | |
|------------------|--|-----------------|-----------------------------------|
| \diamond | node correctly detects Packet A | \bullet | packet sink |
| \boxplus | node correctly detects Packet B | \blacklozenge | source of packet A |
| \diamond_{A_i} | node relays packet A in its i th hop | \blacksquare | source of packet B |
| \boxplus_{B_i} | node relays packet B in its i th hop | — | relaying strip borders (packet A) |
| + | node not part of relaying process | — | relaying strip borders (packet B) |

(b) Legend

Fig. 14. Demonstrating the flow of two concurrent packets in the network under OMR.

TABLE I
TYPICAL ENERGY CONSUMPTION COMPONENTS FOR A BEACONLESS PROTOCOL.

| η empty cycles | | | |
|---------------------|---|---|----------------|
| Node(s) | Count | Activity | Duration |
| sender | 1 | transmit RTS | T_s |
| | | listening and activating BT while listening | $\eta N_p T_s$ |
| | | transmits CONTINUE message after each slot not containing CTS | $\eta N_p T_s$ |
| non-empty cycle | | | |
| Node(s) | Average Count | Activity | Duration |
| sender | 1 | transmit RTS | T_s |
| sender | 1 | listening and activating BT while listening | $m_e T_s$ |
| | | transmits CONTINUE message after each slot not containing CTS | $m_e T_s$ |
| potential relays | $\frac{(N_p - m_e)}{N_p} \xi \epsilon \rho \pi d_m^2$ | listen to the channel in anticipation of a CTS message | $m_e T_s$ |
| | | listen to CONTINUE messages from sender | $m_e T_s$ |
| | | activate BT while listening | $2m_e T_s$ |
| timers expired | $\frac{\xi \epsilon \rho \pi d_m^2}{N_p}$ | transmit CTS message in $(m_e + 1)$ th slot | T_s |
| colliding | at least 2 | transmit CTS, listen for CTS-Reply from sender, activate BT while listening | $(m_n - 1)T_s$ |
| sender | 1 | transmit CONTINUE message | $(m_n - 1)T_s$ |
| | | receive colliding CTS messages | $(m_n - 1)T_s$ |
| successful relay | 1 | transmit CTS message during $(m_e + m_n)$ th slot | T_s |
| sender | 1 | listen to CTS from successful relay during $(m_e + m_n)$ th slot | T_s |
| | | activate BT while listening | T_s |
| | | transmit OK message | T_s |
| successful relay | 1 | listen to OK message and activate BT while listening | T_s |